Advances in Radiation Oncology (2025) **10**, 101661

advances in radiation oncology

www.advancesradonc.org

Scientific Article

Optimal Setup and Parameters of Diffusion-Weighted Magnetic Resonance Imaging for Translational Evaluation of a Tumor Progression Model for Soft Tissue Sarcomas

Nadya Shusharina, PhD,[a,b,*] Stephan E. Maier, MD, PhD,[b,c] Miranda B. Lam, MD, MBA,[b,d,e] and Evangelia Kaza, PhD[b,d,e]

[a]Division of Radiation Biophysics, Department of Radiation Oncology, Massachusetts General Hospital, Boston, Massachusetts; [b]Harvard Medical School, Boston, Massachusetts; [c]Department of Radiology, Brigham and Women's Hospital, Boston, Massachusetts; [d]Department of Radiation Oncology, Brigham and Women's Hospital, Boston, Massachusetts; and [e]Dana-Farber Cancer Institute, Boston, Massachusetts

Received 19 February 2024; accepted 8 October 2024

Purpose: Defining a microscopic tumor infiltration boundary is critical to the success of radiation therapy. Currently, radiation oncologists use margins to geometrically expand the visible tumor for radiation treatment planning in soft tissue sarcomas (STS). Image-based models of tumor progression would be critical to personalize the treatment radiation field to the pattern of sarcoma spread. Evaluation of these models is necessary to demonstrate feasibility in the clinical setting. This study presents an imaging protocol for the preclinical evaluation of a tumor progression model in extremity STS.

Methods and Materials: We recruited 7 healthy volunteers and acquired diffusion-weighted magnetic resonance imaging (DW-MRI) images of the thigh on a magnetic resonance imaging scanner used for imaging cancer patients in a radiation oncology department. We developed a protocol that includes positioning the patient, configuring the radiofrequency coils, and setting the DW-MRI sequence parameters. To find the optimal parameter configuration, the image signal-to-noise ratio (SNR) and the directional variability (DV) of the principal eigenvector of the diffusion tensor were calculated.

Results: The mean SNR across all trials and 12 thigh muscles was 41, with a range of 12 to 72. The mean DV was 13° and ranged from 11° to 23°. The longest scan time was 22 minutes and 58 seconds, and the shortest was 11 minutes and 46 seconds. For the high-resolution image with a voxel volume of $1.3 \times 1.3 \times 6$ mm^3 and 38 slices, the optimal parameters were found to be a repetition time of 8000 ms, 12 signal averages, and 6 gradient directions. This configuration resulted in a scan time of 11 minutes and 46 seconds, an SNR of 34, and a DV of 13°.

Conclusions: A DW-MRI scan duration acceptable for imaging cancer patients was achieved with an image quality suitable for reproducible modeling of tumor infiltration. The developed protocol can be used for preclinical evaluation in STS patients.

Sources of support: This research was supported by the National Cancer Institute Grant (R01CA241817), the National Institute of Biomedical Imaging and Bioengineering (R03EB030831), and the National Institute of Biomedical Imaging and Bioengineering Grant (P41EB028741).

Research data are not available at this time.

*Corresponding author: Nadya Shusharina, PhD; Email: nshusharina@mgh.harvard.edu

https://doi.org/10.1016/j.adro.2024.101661

Introduction

More than 13,500 new cases of soft tissue sarcoma (STS) are expected to be diagnosed in the United States in 2024, resulting in approximately 5200 deaths.[1] The majority of deaths from STS occur in the 14- to 29-year age group[2,3] because of common recurrence, and therefore, improved treatments are urgently needed, especially limb-sparing local treatments. However, the development of improved radiation therapy (RT) techniques for STS is more challenging than for other cancers because of the relative rarity of this disease.[4] Randomized trials have shown that the combination of RT and surgery results in better local control rates than surgery alone.[5] Equivalent local control rates were shown whether RT was given preoperatively or postoperatively.[6] However, there are differences in the side effect profiles of the 2 options. Preoperative RT is associated with higher rates of wound complications compared with postoperative RT (35% vs 17%). Postoperative RT requires a higher total RT dose (60-66 Gy vs 50 Gy) and a larger treatment volume to cover the surgical bed, leading to higher rates of fibrosis, edema, joint stiffness, and functional limitations that are thought to be permanent.[6-8]

Further studies are needed to determine the best treatment option for STS, with the goal of reducing both recurrence rates and treatment complications. Standardization of the clinical target volume (CTV) definition to exclude factors related to different practice-specific spatial/anatomic localization of high radiation doses is critical for the success of clinical trials. However, defining the CTV boundary remains a matter of clinical judgment, subject to variability in expert opinion.[9-14] With a standardized definition of the CTV, analysis of the results of clinical trials will be simplified, and the failure rate in the later stages of validation will be reduced.

Although microscopic tumor spread is not visible in medical imaging, it is still possible to provide an evidence-based definition of where it is limited. Recent microscopic studies have confirmed that tumor cells invade soft tissue by adapting to the encountered tissue structure, specifically along muscle fibers.[15,16] As morphologic magnetic resonance (MR) or computed tomography (CT) imaging cannot resolve muscle fibers, other imaging modalities should be investigated and brought to the clinic. It is well established that diffusion-weighted (DW) MR imaging (DW-MRI) can quantitatively describe the directionality of muscle fibers. The diffusion tensor quantifies the anisotropic diffusion of water in the interfiber space.[17-22] The principal eigenvector of the tensor, corresponding to the largest eigenvalue, is parallel to the dominant orientation of the muscle fibers and reflects their local directionality; therefore, the parameters derived from DW-MRI data can be used to inform CTV delineation.

Recently, a model for quantifying tumor spread in soft tissue has been proposed that uses anisotropic geodesics to infer muscle fiber trajectories directly from DW data without recourse to classical tractography.[23] Using this model, it is possible to define the boundary of microscopic tumor spread on a pretreatment DW-MRI scan. Implementation of this method requires preclinical development and validation. The accuracy of defining the boundary of microscopic tumor spread depends critically on the reproducibility and quality of the DW-MRI data.[19,24]

The contributions of this study are as follows:

- We investigate DW-MRI imaging setup parameters in healthy volunteers in preparation for future studies in STS patients. We focus on achieving image quality that adequately estimates the diffusion tensor in muscle, allowing for accurate and reproducible modeling of sarcoma spread in muscle.
- The criterion we use is minimal variability in the direction of the principal eigenvector while maintaining a high signal-to-noise ratio (SNR) for the high image resolution.
- We establish recommendations for positioning, immobilization, coil configuration, sequence parameters, and acquisition time to be translated into a clinically applicable protocol.

Methods and Materials

Subjects

Healthy volunteer MR scans and analysis of obtained data were approved by the institutional review boards of the participating institutions. Written informed consent was obtained from each healthy subject.

Seven healthy volunteers (4 males and 3 females) with a mean age of 35 $\pm$ 11 years, a mean weight of 67.4 $\pm$ 9.7 kg, and a mean height of 1.70 $\pm$ 0.10 m were recruited. The inclusion criterion was age over 18 years. Exclusion criteria were leg muscle diseases or injuries.

MR image acquisition

Subjects were scanned on a 3T MRI system (Magnetom Vida, Siemens Healthcare; maximum gradient amplitude 60 mT/m; maximum slew rate 200 T/m/s) in the radiation oncology department. This wide-bore (70 cm) MR scanner uses the same patient immobilization equipment as CT and RT to produce patient images that aid treatment planning. The patient table is equipped with a BioMatrix Spine 32 coil (Siemens Healthineers), on top of which an INSIGHT Overlay (Qfix, Avondale) was laid to create a flat surface for patient positioning, as is done during clinical examinations. Subjects were positioned supine and feet first in the bore,

with their scanned leg supported at the calf by a positioning block. The long axis of the examined thigh was parallel to the axis of the static magnetic field. A flexible Body 18 coil (Siemens Healthineers) was placed over the examined thigh. For the first subject (S1), the flexible coil was placed directly on top of the thighs, as reported in previous studies.[23,25] For all subsequent subjects, the coil was attached to an INSIGHT MR Body Coil Holder (Qfix, Avondale) and suspended over the subjects' thighs.

A DW single-shot 2-dimensional echo-planar imaging sequence was acquired with 2 b-values (b_0 = 50 s/mm^2 and b = 400 s/mm^2). Image acquisition was carried out in axial slice orientation. The slice thickness was set to 6 mm without any gap between slices. Spectral adiabatic inversion recovery was used to suppress the fat signal. Our protocol used 5/8 partial Fourier sampling and a partial phase field of view of 44%. A coil acceleration factor of 2 was used with the generalized autocalibrating partially parallel acquisitions technique[26] with 12 reference lines. Together, these parameters reduced the echo time (TE). In addition, the pixel bandwidth was 1.42 kHz. The sequence parameters that were varied to establish the best protocol are listed in Table 1.

An additional 3-dimensional T1-weighted fast low-angle shot MR sequence was acquired for thigh muscle definition, with a repetition time (TR) of 4.6 ms, TE of 2.77 ms, and 128 axial slices of 2 mm thickness and 1 mm^2 in-plane resolution.

Data processing and analysis

The DW series were resampled to an isotropic voxel size equal to the planar resolution of the acquired DW-MR image. The diffusion tensor was reconstructed using the imaging Python library Diffusion Imaging in Python (DIPY)[27] with the tensor model of Basser et al.[28] In addition, we applied the RESTORE tensor fitting algorithm[29] for the automatic detection of data outliers occurring because of subject motion that may be confounded with the physical properties of the muscle fibers.

SNR

The SNR of DW-MR images was computed as the ratio of the mean signal S_{mean} and the SD of the underlying Gaussian noise σ

$$SNR = \frac{S_{mean}}{\sigma} . \quad (1)$$

The noise σ was computed as a local noise variance in each voxel of a muscle using the DIPY library and employing a local Principal Component Analysis (PCA)-based algorithm.[30] To compute the average magnitude of the DW-MRI signal in each voxel, the data were first averaged over all 6 or 12 repetitions in each gradient direction. The magnitude of the signal S_{mean} was then defined as the root mean square amplitude of all gradient directions in every voxel in each muscle.

Consistency of the principal eigenvector direction

Variation of the derived directionality of the muscle fibers was quantified as the voxel-wise angular deviation from the principal eigenvector, averaged over all voxels within a muscle. The averaging process was performed in the following steps. To remove data degeneracy because of up-down symmetry in the direction of the principal eigenvector, 2 clusters of vectors were detected using k-means, and 1 of the 2 clusters was inverted by reflecting the direction of the vector.[24] The mean vector was then calculated for each muscle. The voxel-by-voxel angle between the eigenvectors was corrected for mirroring, and the mean vector was then calculated. Histograms of voxel-wise deviations were plotted for each muscle, and the mode of the histogram, referred to as directional variability (DV), was reported.

Table 1 Diffusion-weighted magnetic resonance imaging sequence parameters

Parameter	S1	S2	S3	S4	S5		S6				S7	
Signal averages, b	12	12	12	12	12		12	6	12	12	12	12
Gradient directions	12	12	12	12	12		12	12	6	12	6	6
TR, ms	8000	7000	5800	8000	8000		8000	8000	8000	6800	8000	9000
TE, ms	78	52	45	45	45	45	45	45	45	45	45	45
Acquisition matrix	320 × 150	196 × 450	183 × 420	222 × 504	222 × 504	188 × 430	222 × 504	222 × 504	222 × 504	188 × 430	188 × 430	188 × 430
Pixel size, mm^2	1.3 × 1.3	1.4 × 1.4	1.3 × 1.3	3 × 3	3 × 3	1.3 × 1.3	3 × 3	3 × 3	3 × 3	1.3 × 1.3	1.3 × 1.3	1.3 × 1.3
Echo spacing, ms	1.03	0.79	0.96	0.79	0.79	0.96	0.79	0.79	0.79	0.96	0.96	0.96
No. of slices	38	45	38	38	38	38	38	38	38	38	38	38
Acquisition time, min:s	23:04	20:11	16:41	22:58	22:58	22:58	22:58	13:22	11:46	19:32	11:46	13:14

Abbreviations: TE = echo time; TR = repetition time.

Modeling CTV

We employed a recently described algorithm[23] that assumes that individual cancer cells infiltrate tissue with a directional velocity outward from the macroscopic tumor mass. Under this assumption, the boundary of microscopic disease spread can be thought of as a tumor cell propagation front quantified by surfaces of equal-weighted shortest path distance ($\boldsymbol{x}$) (isosurfaces) whose gradient is determined by the spatial distribution of tumor propagation velocities. Propagation stops when a desired distance from the tumor is reached, defining the CTV margin. This is described by the Eikonal equation

$$\| \nabla L(\boldsymbol{x}) \|_{\boldsymbol{M}} = 1, \; L(\boldsymbol{x})\Big|_{\partial\Omega} = 0, \tag{2}$$

where $L(\boldsymbol{x})$ is the shortest distance from the boundary $\partial\Omega$ (the surface of the tumor mass) to the point, and $\|\bullet\|_{\mathbf{M}}$ is the norm with respect to the metric tensor $\boldsymbol{M}$ reconstructed from DW-MRI data. To solve equation (2), we transformed the diffusion tensors reconstructed from the DW-MRI data by keeping their eigenvectors but replacing the eigenvalues (in increasing order) with $\lambda_1 = \lambda_2 = 1$ and $\lambda_3 = 10$. An advantage of this approach over the direct use of the full diffusion tensor is that the choice of λ allows us to tailor the resulting CTV based on clinical experience and to account for differences between water diffusivity and tumor cell spread. To find the isosurfaces of shortest distances, we numerically solved the Eikonal equation in anisotropic media using an open-source implementation of the Hamiltonian Fast-Marching solver.[31,32]

Study design

To determine an acquisition setup that was repeatable between pretreatment imaging and treatment sessions, reliable for applying the tumor propagation model, and comfortable for the cancer patient, we considered the following factors: (1) immobilization of the leg; (2) appropriate selection and positioning of the radiofrequency coils; (3) image quality and resolution; and (4) scan time.

Results

Tissue segmentation

The 12 muscles of the thigh, adductor longus, adductor magnus, biceps femoris long head, biceps femoris short head, gracilis, rectus femoris, sartorius, semimembranosus, semitendinosus, vastus medialis, vastus intermedius, and vastus lateralis, were manually delineated on the T1-weighted images. Figure 1 shows the muscles, femoral bone, subcutaneous fat, and perimuscular tissues for an example subject. The individual muscles were divided into anterior, medial, and posterior compartments. The perimuscular tissues include the intermuscular septum, blood vessels, nerves, and perimuscular fat deposits. The produced muscle masks were used to calculate the SNR and DV of the principal eigenvector.

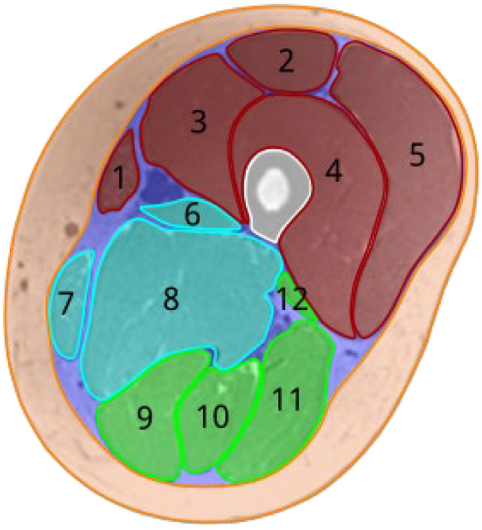

Figure 1 Segmentation of the thigh tissue. Individual muscles in the anterior (red), medial (cyan), and posterior (green) compartments are sartorius (1), rectus femoris (2), vastus medialis (3), vastus intermedius (4), vastus lateralis (5), adductor longus (6), gracilis (7), adductor magnus (8), semimembranosus (9), semitendinosus (10), biceps femoris long head (11), and biceps femoris short head (12). The femoral bone is shown in white. Subcutaneous fat is in orange, and perimuscular tissues are in purple.

Leg immobilization

To avoid muscle deformation because of compression of the thigh against the table, we selected a foam block with a semicylindrical recess supporting the calf (Vanarsdale Innovative Products Inc) as the best option among the available clinically employed leg supports for thigh elevation and immobilization (Fig. 2C). The setup was well reproducible by fixing the position of the block relative to the flatbed edge (Fig. 2D). We found that T1-weighted and DW-MRI signal uniformity was adequate when suspending the top coil ~8 cm from the anterior thigh surface (Fig. 2E). This distance was roughly equal to that of the posterior thigh surface to the bottom coil. All subjects reported that the position was comfortable throughout the acquisition session and that they did not have to move to reposition themselves.

Radiofrequency coils

With a flexible coil directly on top of the thighs for S1 (Fig. 2A), image quality was unsatisfactory, with significant signal nonuniformities; the anterior thigh was brighter, and the posterior was darker because of the different

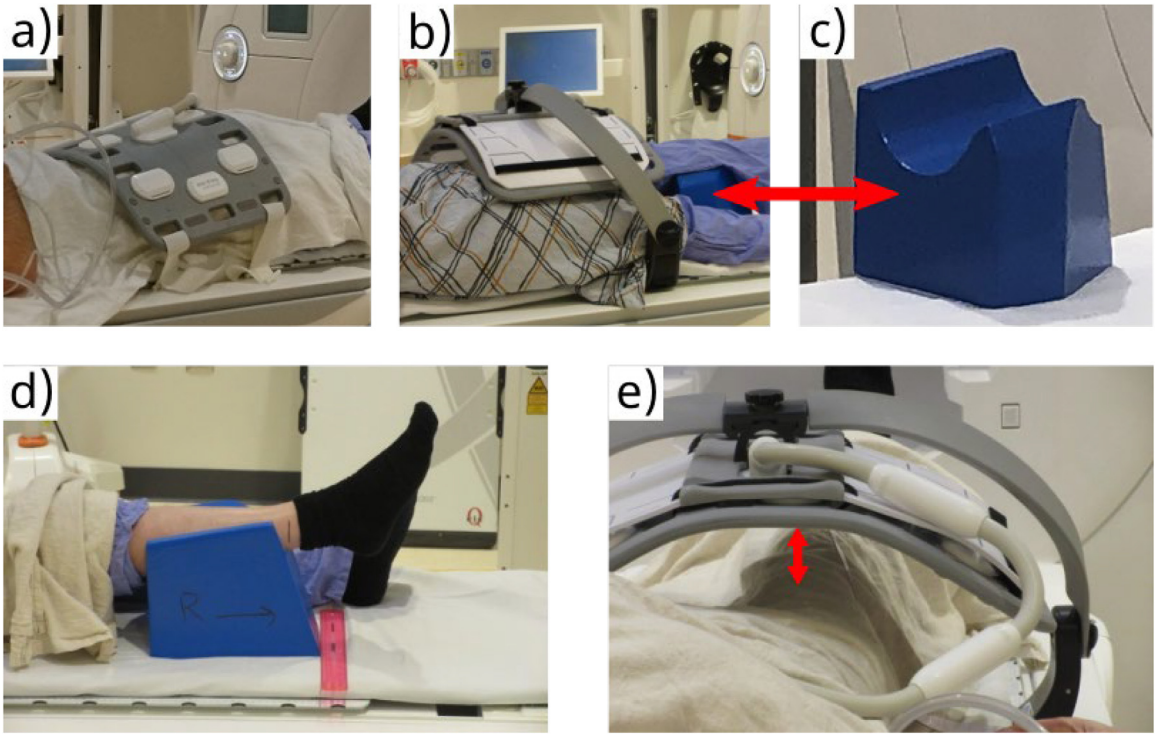

Figure 2 Healthy volunteer setup for thigh magnetic resonance imaging. Radiofrequency coil positioning: (A) flat flexible coil covers both thighs; (B) coil with adapter is positioned over both thighs with the examined leg parallel to the magnet axis. (C) The ankle of the leg under examination is supported by a foam block with a semicylindrical recess (D) placed in a fixed position relative to the flatbed scale; (E) the distance between the surface of the thigh and the coil is measured.

distance of the anterior thigh to the overlying flexible coil and the posterior thigh to the underlying rigid spine coil. Image signal inhomogeneity and the principal eigenvector variability map are shown in Fig. 3, S1. Histograms of the variability per muscle and compartment are also shown.

The SNRs and DVs calculated within each muscle for all subjects are compiled in Table 2. The low uniformity of the images acquired with the Body 18 coil laid flat on the thigh is consistent with them having the lowest SNR (see Table 2, subject S1, mean SNR of 12 and mean DV of 23°, much higher than previously reported[24]). For this reason, we increased the distance of the top coil to the thigh by attaching it to an INSIGHT MR Body Coil Holder for all the subsequent subjects, as shown in Fig. 2B. With the new coil setup, image signal homogeneity was notably improved (see Fig. 3, S5), with the SNR ranging from 49 to 90 for different muscles (mean, 65 ± 13). The variability of the principal eigenvector direction was also reduced, with a mean DV of 10° (see Table 2).

DW-MR image quality and scan time

Here, we searched for the optimal parameter configuration to find the best tradeoff between image quality and scan time. We evaluated the image quality in terms of SNR and DV. As the reference, we chose a coarse voxel grid with a voxel size of $3 \times 3 \times 6$ mm^3, a TE of 45 ms, a TR of 8000 ms, 12 signal averages, and 12 gradient directions (see Table 1). The acquisition time was almost 23 minutes, with an SNR of 65 and a DV of 10°.

For accurate CTV boundary definition, the model must be applied to a fine-grained image grid. The scan for subject S5 was repeated, keeping all parameters the same and increasing the lateral resolution to a pixel size of 1.3×1.3 mm^2. As expected, the SNR decreased almost 2-fold with a range from 24 to 43 (mean, 33 ± 6), while the DV increased from 10° to 12° (Table 2, subject S5). The scan time did not change and remained at 23 minutes.

To reduce the scan time, we could either reduce the TR, the number of signal averages, or the number of gradient directions. By reducing the TR to 6800 ms, we obtained an SNR of 29 and a DV of 14°, but the scan time was only reduced to 19 minutes and 32 seconds (Tables 1 and 2, subject S6). We then reduced the number of signal averages to 6, resulting in a scan time of 13 minutes and 22 seconds. The shortest scan time (11 minutes and 46 seconds) was observed when the number of gradient directions was reduced to 6, with an SNR of 34 and a DV of 13°. In Table 1, the set of parameters for this optimal configuration is shaded green. Figure 4 summarizes the search in the sequence parameter space, with the arrow denoting the optimal configuration.

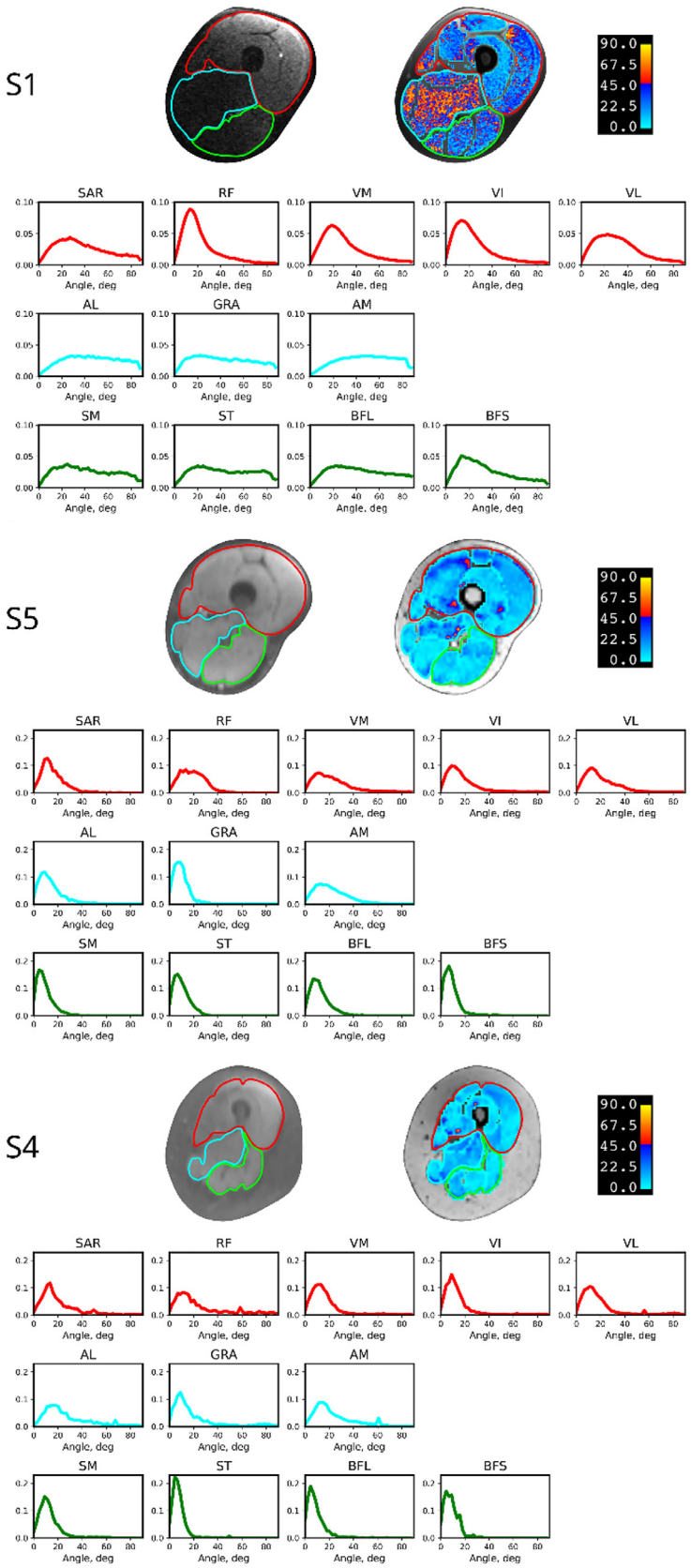

Figure 3 Diffusion-weighted magnetic resonance image and the principal eigenvector variability map of subjects S1, S5, and S4. S1 was scanned with the flexible radiofrequency coil placed on the top of the thigh, as shown in Fig. 2A. S5 and S4 were scanned with the

Effect of subcutaneous fat

To investigate the effect of the presence of subcutaneous fat on image quality, we imaged a subject with a thick layer of subcutaneous fat (Fig. 3, S4) using the same sequence parameters as were used for a subject with a much thinner layer. The SNR and DV were very similar (see S5 and S4 in Table 2), suggesting that the thickness of subcutaneous fat has no appreciable effect on DW-MR image quality for a given sequence.

Model calculations

Using DW-MRI data obtained with the optimal acquisition setup parameter configuration, we reconstructed the voxel-wise diffusion tensor and used it as input for the Eikonal equation (2). The solutions of the equation are the shortest path isosurfaces from the muscle center, as shown in Fig. 5. A qualitative visual inspection of the isosurfaces in the 5 muscles showed different directionality of the fibers, suggesting that the shape of the CTV boundary depends on the location of the tumor, and therefore patient-specific image-based CTV definition will be superior to currently used methods.

Discussion

Our study provides guidelines for preclinical validation of the CTV delineation model for muscle abnormalities; cancer imaging requires a shorter acquisition time and a more consistent direction of the principal eigenvector of the diffusion tensor to precisely define the directionality of muscle fibers. Furthermore, higher DW-MRI image resolution is desirable to match the resolution of the planning CT or morphologic MRI scan. Here, patient and acquisition setup parameters and their influence on DW-MRI data quality were investigated to achieve these requirements.

Many radiation oncology departments have chosen to dedicate an MRI scanner as an MR simulator to acquire patient images in the treatment position.[33] This is achieved by placing flat covers on the scanner couch on which immobilization masks are mounted. Due to the masks, the rigid coils designed to maximize SNR and signal uniformity for a specific body part (eg, head, knee, and foot coils) cannot be used. MR simulators employ flexible surface coils instead, which can be wrapped around the immobilization masks. The surface coils provide maximum SNR at a distance similar to the diameter of their individual elements.[34] In our study, we considered the distance of the flat couch overlay to the lower spinal coil and the distance of the elevated thigh to the overlay to determine the required distance of the upper coil to the thigh. Our proposed leg placement and coil configuration were reproducible and well tolerated by all participating subjects.

The findings of our study will inform the design of future clinical trials investigating novel therapeutic approaches for STS. For instance, it could be a valuable contribution to the recently published protocol for habitat escalated adaptive therapy,[35] which combines genomics and radiomics to personalize STS RT. In addition to the standard CT and MR scans, the habitat escalated adaptive therapy protocol employs a pretreatment DW-MRI to determine the radiomic habitats within the gross tumor volume. Our method can be used to define the CTV using the same sequence, thus better conforming the RT target to the anatomic compartments and standardizing the CTV definition.

As shown by previous studies on the reproducibility of the diffusion tensor-derived measures, DW-MRI data are generally reproducible.[36-39] The SNR affects both eigenvectors and eigenvalues simultaneously.[19] However, the tumor propagation model[23] assumes preferential propagation along the muscle fibers. Accordingly, instead of using the full diffusion tensor, the fiber orientation is approximated by the principal eigenvector of the tensor. The eigenvalues of the tensor are not used in this study and are replaced by [10,1,1] to model the different degrees of tumor propagation asymmetry. Therefore, our focus in this study was on the directional stability of the principal eigenvector.

Our study confirms that a higher SNR is required for better stability of the principal eigenvector. At high image resolution, SNR can be increased at the cost of acquisition time. The tradeoff between TR, number of signal averages, and number of gradient directions was achieved at a TR of 8000 ms with 12 averages and 6 gradient directions. For the optimal parameter configuration, the imaging protocol had a scan duration of 11 minutes and 46 seconds, which we anticipate will be generally well tolerated by cancer patients.

Compared with brain tissue, which has a T_2 relaxation time of 70 ms at 3T, muscle T_2 relaxation time is twice as short, making the b-value of 1000 s/mm^2 used in brain studies suboptimal for soft tissue.[40,41] In the soft tissue simulation, the optimal b-value for accurate reconstruction of diffusion tensor parameters was determined by

coil with a bridge adapter, as shown in Fig. 2B. The red, cyan, and green borders indicate the anterior, middle, and posterior muscle compartments, respectively. The histograms of variability in the direction of the principal eigenvector are plotted for each muscle and divided by compartment. The color of the histogram represents the color of the corresponding compartment.

Abbreviations: AL = adductor longus; AM = adductor magnus; BFL = biceps femoris long head; BFS = biceps femoris short head; GRA = gracilis; RF = rectus femoris; SAR = sartorius; SM = semimembranosus; ST = semitendinosus; VI = vastus intermedius; VL = vastus lateralis; VM = vastus medialis.

Table 2 Signal-to-noise ratio and directional variability within each muscle at different parameters. Colors represent anterior (red), medial (cyan), and posterior (green) compartments

Muscle	S1		S2		S3		S4		S5				S6								S7			
Pixel, mm^2	1.3 × 1.3		1.4 × 1.4		1.3 × 1.3		3 × 3		3 × 3		1.3 × 1.3		3 × 3						1.3 × 1.3		1.3 × 1.3		1.3 × 1.3	
Averages	12		12		12		12		12				12		6		12		12		12			
Directions	12		12		12		12		12				12		12		6		12		6			
TR, ms	8000		7000		5800		8000		8000				8000						6800		8000		9000	
	SNR	DV	SNR	DV	SNR	DV	SNR	DV	SNR	DV	SNR	DV	SNR	DV	SNR	DV	SNR	DV	SNR	DV	SNR	DV	SNR	DV
SAR	9.7	27.0	10.0	32.5	14.6	18.0	50.9	13.0	57.2	10.0	34.0	14.0	51.4	20.0	38.4	22.0	49.0	24.0	24.0	16.0	29.4	14.0	26.8	10.0
RF	24.3	14.0	16.0	37.4	20.1	24.0	86.4	11.0	89.7	14.0	43.9	16.0	90.8	28.0	61.6	24.0	72.2	10.0	30.2	16.0	49.3	18.0	46.8	14.0
VM	15.9	20.0	14.0	37.5	15.8	19.0	69.2	13.0	64.2	12.0	34.2	17.0	69.7	8.0	55.3	8.0	63.7	8.0	33.0	16.0	32.0	18.0	31.2	14.0
VI	15.1	15.0	11.0	26.2	16.9	14.0	83.4	10.0	63.3	10.0	33.2	12.0	80.9	10.0	62.8	12.0	72.4	12.0	32.7	16.0	32.9	12.0	34.0	14.0
VL	20.4	25.0	15.0	28.6	18.0	21.0	106.5	13.0	84.5	12.0	43.0	12.0	103.4	12.0	79.2	10.0	90.2	14.0	37.8	16.0	40.2	16.0	41.8	18.0
AL	9.1	29.0	14.0	28.8	9.8	38.0	41.6	20.0	49.6	10.0	25.0	14.0	59.5	8.0	37.3	14.0	44.4	12.0	28.6	16.0	33.1	14.0	26.4	14.0
GRA	8.7	23.0	15.0	25.6	12.8	16.0	58.7	9.0	52.8	11.0	23.7	10.0	53.0	10.0	38.9	14.0	44.8	4.0	23.7	16.0	27.1	14.0	28.4	14.0
AM	8.7	38.0	19.0	23.8	12.9	28.0	55.0	14.0	53.1	15.0	28.3	20.0	55.9	16.0	36.9	18.0	44.9	16.0	25.4	14.0	27.0	16.0	26.5	16.0
SM	7.5	26.0	14.0	28.0	17.8	11.0	76.6	10.0	67.8	7.0	35.3	9.0	42.6	8.0	36.7	12.0	36.0	14.0	27.1	12.0	32.8	12.0	33.7	10.0
ST	8.3	20.0	10.0	27.8	19.3	10.0	75.9	6.0	76.9	7.0	37.5	8.0	59.7	4.0	44.6	8.0	55.1	6.0	27.9	8.0	26.7	10.0	28.8	10.0
BFL	9.4	24.0	14.0	23.2	17.0	15.0	65.0	5.0	67.2	7.0	34.6	13.0	70.0	12.0	55.9	10.0	67.1	8.0	33.9	12.0	40.8	8.0	42.0	10.0
BFS	9.8	15.0	9.0	21.1	16.3	10.0	90.5	5.0	49.4	7.0	28.4	7.0	51.5	6.0	42.6	6.0	49.8	8.0	28.6	8.0	36.9	6.0	39.2	6.0
Mean	12.2	21.3	12.5	28.4	16.0	17.5	71.6	10.2	64.7	9.8	33.4	12.1	65.7	11.8	49.2	13.2	57.5	11.3	29.4	13.8	34.0	13.2	33.8	12.5
SD	5.5	9.0	4.2	5.2	3.0	9.0	18.6	4.5	13.4	3.0	6.3	4.3	18.1	6.7	13.7	5.6	15.8	5.3	4.3	3.1	6.8	3.8	7.1	3.3

Abbreviations: AL = adductor longus; AM = adductor magnus; BFL = biceps femoris long head; BFS = biceps femoris short head; DV = directional variability; GRA = gracilis; RF = rectus femoris; SAR = sartorius; SM = semimbranosus; SNR = signal-to-noise ratio; ST = semitendinosus; TR = repetition time; VI = vastus intermedius; VL = vastus lateralis; VM = vastus medialis.

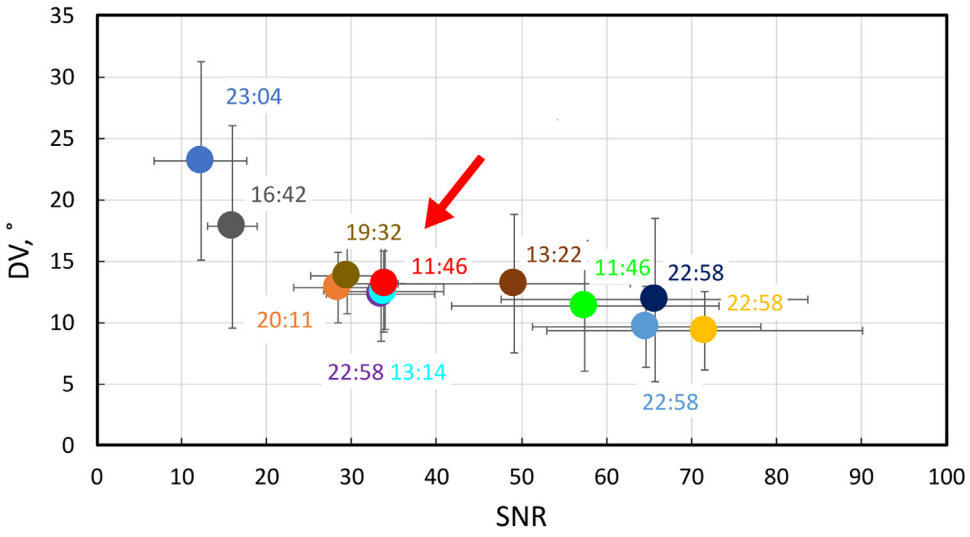

Figure 4 Signal-to-noise ratio (SNR) plotted against directional variability (DV) calculated for each experimental point. The labels indicate the scan time. The arrow points to the optimal configuration.

searching in the range of 50 to 1000 s/mm^2. It has been reported that the error of diffusion tensor eigenvectors was minimal, with a b-value between 400 and 500 s/mm^2 and a resulting echo time between 42 and 45 ms.[42,43] In our study, the largest b-value used was 400 s/mm^2, which increases the signal by approximately 50% compared with using a b-value of 1000 s/mm^2.

The DW-MRI acquisition protocol was optimized using a cohort of healthy volunteers. Since we have taken into account the specificities of imaging cancer patients, it is directly translatable to the clinic. In future studies of STS patients, we will further optimize the protocol by considering parameters that are important for different histologic sarcoma subtypes. For example, for STS

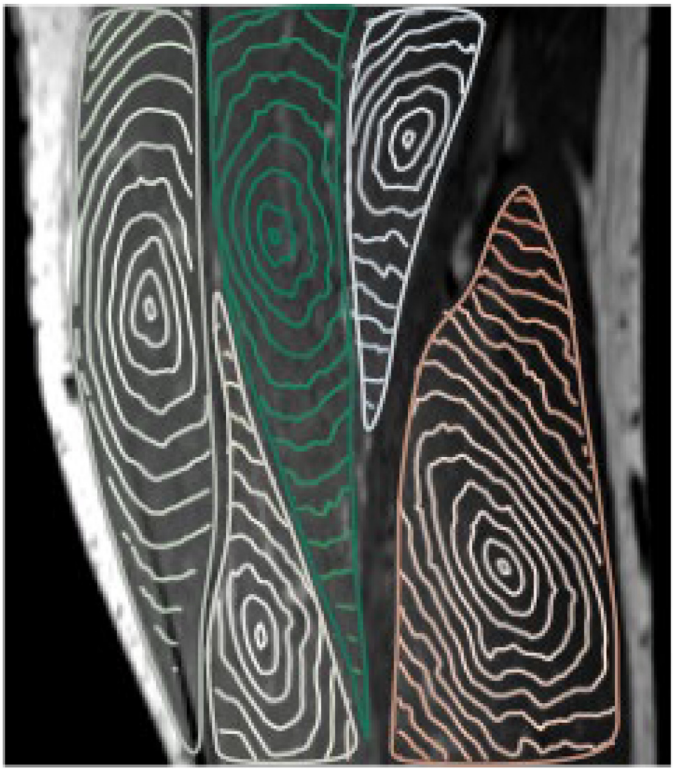

Figure 5 Isosurfaces of the shortest path within muscles starting from a point in the center of each muscle calculated from diffusion-weighted magnetic resonance imaging data acquired with the optimal configuration of parameters.

subtypes derived from adipose tissue, such as myxoid liposarcoma, we will focus on fat suppression techniques to optimize the performance of DW-MRI sequences.

Conclusion

In this study, we performed multiple imaging sessions to develop a protocol for preclinical validation of a sarcoma spread model using DW-MRI data. We considered the effect of MRI sequence parameters on SNR and principal eigenvector stability to achieve optimal imaging data quality and scan duration. Our study provides recommendations for the future implementation of the model for the definition of CTV in patients with sarcoma.

Disclosures

Stephan E. Maier holds US Patents US 2022/0179025A1, US 2022/0034985A1, US 2023/0152406A1, and US 2023/0296711A1, and a stock in GE Medical Systems.

Acknowledgments

We gratefully acknowledge the editorial support of Barclay Lee of the Editorial Support Program at Dana-Farber Cancer Institute in preparing this manuscript. We thank Dr Atchar Sudhyadhom for sharing his expertise and accommodating our study.

References

1. American Cancer Society. https://www.cancer.org. Accessed August 26, 2024.
2. Burningham Z, Hashibe M, Spector L, Schiffman JD. The epidemiology of sarcoma. *Clin Sarcoma Res*. 2012;2:14.
3. Mankin HJ, Lange TA, Spanier SS. THE CLASSIC: The hazards of biopsy in patients with malignant primary bone and soft-tissue tumors. *Clin Orthop Relat Res*. 2006;450:4-10.
4. Haas RL, DeLaney TF, O'Sullivan B, et al. Radiotherapy for management of extremity soft tissue sarcomas: Why, when, and where? *Int J Radiat Oncol Biol Phys*. 2012;84:572-580.
5. Rosenberg SA, Tepper J, Glatstein E, et al. The treatment of soft-tissue sarcomas of the extremities: Prospective randomized evaluations of (1) limb-sparing surgery plus radiation therapy compared with amputation and (2) the role of adjuvant chemotherapy. *Ann Surg*. 1982;196:305-315.
6. O'Sullivan B, Davis AM, Turcotte R, et al. Preoperative versus postoperative radiotherapy in soft-tissue sarcoma of the limbs: A randomised trial. *Lancet*. 2002;359:2235-2241.
7. Cannon CP, Ballo MT, Zagars GK, et al. Complications of combined modality treatment of primary lower extremity soft-tissue sarcomas. *Cancer*. 2006;107:2455-2461.
8. Davis AM, Sennik S, Griffin AM, et al. Predictors of functional outcomes following limb salvage surgery for lower-extremity soft tissue sarcoma. *J Surg Oncol*. 2000;73:206-211.
9. Vinod SK, Jameson MG, Min M, Holloway LC. Uncertainties in volume delineation in radiation oncology: A systematic review and recommendations for future studies. *Radiother Oncol*. 2016;121:169-179.
10. Cloak K, Jameson MG, Paneghel A, et al. Contour variation is a primary source of error when delivering post prostatectomy radiotherapy: Results of the Trans-Tasman Radiation Oncology Group 08.03 Radiotherapy Adjuvant Versus Early Salvage (RAVES) benchmarking exercise. *J Med Imaging Radiat Oncol*. 2019;63:390-398.
11. Genovesi D, Ausili Cefaro G, Trignani M, et al. Interobserver variability of clinical target volume delineation in soft-tissue sarcomas. *Cancer Radiother*. 2014;18:89-96.
12. Hong TS, Tomé WA, Harari PM. Heterogeneity in head and neck IMRT target design and clinical practice. *Radiother Oncol*. 2012;103:92-98.
13. Wang D, Bosch W, Kirsch DG, et al. Variation in the gross tumor volume and clinical target volume for preoperative radiotherapy of primary large high-grade soft tissue sarcoma of the extremity among RTOG sarcoma radiation oncologists. *Int J Radiat Oncol Biol Phys*. 2011;81:e775-e780.
14. Njeh CF. Tumor delineation: The weakest link in the search for accuracy in radiotherapy. *J Med Phys*. 2008;33:136-140.
15. Weigelin B, Bakker GJ, Friedl P. Intravital third harmonic generation microscopy of collective melanoma cell invasion. *IntraVital*. 2012;1:32-43.
16. Weigelin B, Bakker GJ, Friedl P. Third harmonic generation microscopy of cells and tissue organization. *J Cell Sci*. 2016;129:245-255.
17. Damon BM, Froeling M, Buck AK, et al. Skeletal muscle DT-MRI fiber tracking: Rationale, data acquisition and analysis methods, applications, and future directions. *NMR Biomed*. 2017;30. https://doi.org/10.1002/nbm.3563.
18. Berry DB, Regner B, Galinsky V, Ward SR, Frank LR. Relationships between tissue microstructure and the diffusion tensor in simulated skeletal muscle. *Magn Reson Med*. 2018;80:317-329.
19. Rockel C, Noseworthy MD. An exploration of diffusion tensor eigenvector variability within human calf muscles. *J Magn Reson Imaging*. 2016;43:190-202.
20. Budzik JF, Le Thuc V, Demondion X, Morel M, Chechin D, Cotten A. In vivo MR tractography of thigh muscles using diffusion imaging: Initial results. *Eur Radiol*. 2007;17:3079-3085.
21. Lansdown DA, Ding Z, Wadington M, Hornberger JL, Damon BM. Quantitative diffusion tensor MRI-based fiber tracking of human skeletal muscle. *J Appl Physiol (1985)*. 2007;103:673-681.
22. Bihan DL, Iima M. Diffusion magnetic resonance imaging: What water tells us about biological tissues. *PLoS Biol*. 2015;13: e1002203.
23. Shusharina N, Liu X, Coll-Font J, et al. Feasibility study of clinical target volume definition for soft-tissue sarcoma using muscle fiber orientations derived from diffusion tensor imaging. *Phys Med Biol*. 2022;67. https://doi.org/10.1088/1361-6560/ac8045.
24. Shusharina N, Nguyen C. Consistency of muscle fibers directionality in human thigh derived from diffusion-weighted MRI. *Phys Med Biol*. 2023;68: 175045.
25. Weygand J, Armstrong T, Bryant JM, et al. Accurate, repeatable, and geometrically precise diffusion-weighted imaging on a 0.35 T magnetic resonance imaging-guided linear accelerator. *Phys Imaging Radiat Oncol*. 2023;28: 100505.
26. Griswold MA, Jakob PM, Heidemann RM, et al. Generalized autocalibrating partially parallel acquisitions (GRAPPA). *Magn Reson Med*. 2002;47:1202-1210.
27. Garyfallidis E, Brett M, Amirbekian B, et al. Dipy, a library for the analysis of diffusion MRI data. *Front Neuroinform*. 2014;8:8.
28. Basser PJ, Mattiello J, LeBihan D. MR diffusion tensor spectroscopy and imaging. *Biophys J*. 1994;66:259-267.
29. Chang L-C, Jones DK, Pierpaoli C. RESTORE: Robust estimation of tensors by outlier rejection. *Magn Reson Med*. 2005;53:1088-1095.

30. Manjón JV, Coupé P, Concha L, Buades A, Collins DL, Robles M. Diffusion weighted image denoising using overcomplete local PCA. *PloS One*. 2013;8:e73021.
31. Mirebeau JM, Portegies J. Hamiltonian fast marching: A numerical solver for anisotropic and non-holonomic eikonal PDEs. *Image Process Line*. 2019;9:47-93.
32. Mirebeau JM. Riemannian fast-marching on cartesian grids, using Voronoi's first reduction of quadratic forms. *SIAM J Numer Anal*. 2019;57:2608-2655.
33. van der Heide UA, Frantzen-Steneker M, Astreinidou E, Nowee ME, van Houdt PJ. MRI basics for radiation oncologists. *Clin Transl Radiat Oncol*. 2019;18:74-79.
34. Roemer PB, Edelstein WA, Hayes CE, Souza SP, Mueller OM. The NMR phased array. *Magn Reson Med*. 1990;16:192-225.
35. Naghavi AO, Bryant JM, Kim Y, et al. Habitat escalated adaptive therapy (HEAT): A phase 2 trial utilizing radiomic habitat-directed and genomic-adjusted radiation dose (GARD) optimization for high-grade soft tissue sarcoma. *BMC Cancer*. 2024;24:437.
36. Heemskerk AM, Sinha TK, Wilson KJ, Ding Z, Damon BM. Repeatability of DTI-based skeletal muscle fiber tracking. *NMR Biomed*. 2010;23:294-303.
37. Sinha S, Sinha U. Reproducibility analysis of diffusion tensor indices and fiber architecture of human calf muscles in vivo at 1.5 Tesla in neutral and plantarflexed ankle positions at rest. *J Magn Reson Imaging*. 2011;34:107-119.
38. Froeling M, Oudeman J, van den Berg S, et al. Reproducibility of diffusion tensor imaging in human forearm muscles at 3.0 T in a clinical setting. *Magn Reson Med*. 2010;64:1182-1190.
39. Monte JR, Hooijmans MT, Froeling M, et al. The repeatability of bilateral diffusion tensor imaging (DTI) in the upper leg muscles of healthy adults. *Eur Radiol*. 2020;30:1709-1718.
40. Stanisz GJ, Odrobina EE, Pun J, et al. T1, T2 relaxation and magnetization transfer in tissue at 3T. *Magn Reson Med*. 2005;54:507-512.
41. Wansapura JP, Holland SK, Dunn RS, Ball Jr WS. NMR relaxation times in the human brain at 3.0 tesla. *J Magn Reson Imaging*. 1999;9:531-538.
42. Froeling M, Nederveen AJ, Nicolay K, Strijkers GJ. DTI of human skeletal muscle: The effects of diffusion encoding parameters, signal-to-noise ratio and T2 on tensor indices and fiber tracts. *NMR Biomed*. 2013;26:1339-1352.
43. Damon BM. Effects of image noise in muscle diffusion tensor (DT)-MRI assessed using numerical simulations. *Magn Reson Med*. 2008;60:934-944.